

IMECE2002-33173

DIGITAL HOLOGRAPHIC PIV FOR 3D FLOW MEASUREMENT

Gang Pan and Hui Meng
Department of Mechanical and Aerospace Engineering
State University of New York at Buffalo
Buffalo, NY 14260

ABSTRACT

We have developed a simple digital holographic PIV system for 3D measurement of turbulent and multiphase flow. This system records in-line holograms of tracer particles directly on a digital camera and reconstructs the 3D particle field numerically. Using a novel complex amplitude-based method, we are able to overcome the depth of focus problem and the speckle noise problem associated with the low resolution of digital sensors and the in-line holographic setup. In this paper we will give detailed description of our system, and present the preliminary result of the benchmark experiment using a water jet.

1. INTRODUCTION

Particle image velocimetry (PIV) has become a widely used technique for velocity measurement in many applications involving fluid flow. Conventional PIV systems can only provide two-dimensional (2D) velocity vectors in a single plane, which is insufficient to answer many challenging questions in fluid dynamics concern complex three-dimensional (3D) flow. Efforts have been made on extending the spatial range of PIV technique to the third dimension. Among various extensions of 2D PIV, stereoscopic PIV is the most common and systems based on Scheimpflug configuration [1] are nowadays commercially available to provide 3-component velocity measurement. Unfortunately stereoscopic PIV is inherently confined to a single plane, and hence it is considered a quasi-3D technique although several approaches have been proposed to enable multiple plane measurement of stereoscopic PIV [2, 3]. Defocusing digital particle image velocimetry (DDPIV) [4] is another extension of PIV technique, which relies on multiple apertures to retrieve depth information. Unlike stereoscopic PIV, DDPIV is capable of measuring instantaneous 3D velocity field in a fairly large volume. But particle seeding density is very much limited with this technique.

Holographic PIV [5] has been recognized as the most thorough approach for instantaneous, volumetric 3D measurement of flow velocity field. Unlike photography-based

PIV systems, holographic PIV records the 3D information of tracer particles in a fluid *volume* instantaneously by capturing the phase information of light waves scattered off the particles, and then reconstructs the "frozen" particle images in a 3D space. From the reconstructed image field, one can retrieve the 3D positions of these particles. By finding the 3D displacements of the tracer particles in the image volume between two exposures separated by a very brief time lapse, the instantaneous 3D velocity field of the flow can be obtained.

The silver-halide-based holographic film, which offers a superior resolution (typically 5000 line pairs per mm), is usually chosen to perform volumetric recording in holographic PIV. Unfortunately, the holographic films require chemical developing and fixing, a process increasingly viewed as undesirable by potential users. Furthermore, the optical reconstruction requires tedious 3D mechanical scanning of the reconstructed image volume, a process that takes up most of the data processing time. As a result, most holographic PIV systems [6-9] are restricted to single-shot, and cinematic holographic PIV [10] to provide temporal measurements remains an unfulfilled promise.

To circumvent the drawbacks associated with film-based recording and optical reconstruction, we have developed a fully digital holographic PIV system. With the digital holographic approach [11], holograms are directly recorded on a digital camera and reconstructed numerically [12]. This not only eliminates wet chemical processing and mechanical scanning but also allows flexible reconstruction algorithms to achieve optimization of specific information. Furthermore, digital holography greatly simplifies the hardware setup for cinematic holographic recording and reconstruction, hence making cinematic implementation of holographic PIV much easier.

Despite these promising prospects, digital holographic PIV is inherently limited by the poor resolution of solid-state image sensors. Currently the smallest pixel size of scientific CCD sensors is around 4 μm , compared with the silver-halide holographic films with an equivalent pixel size down to 0.1 μm . Since the digital sensor elements cannot resolve interference fringes finer than the pixel size, the permissible angle between

object wave and reference wave is limited to a few degrees. Consequently the numerical aperture of a particle hologram is limited to be less than 0.1. The small numerical aperture leads to a remarkably large depth of focus in the reconstructed particle images, which severely compromises the 3D capability of digital holography. Moreover, the small aperture makes the intrinsic speckle noise in particle holography more of a problem. As a result, with digital holographic PIV it is difficult to attain high particle seeding density and thick sample volume at the same time.

As an undertake of the problem, we developed a simple digital holographic PIV system based on in-line holography and forward light scattering. This system records in-line holograms of tracer particles directly on a digital camera and reconstructs the 3D particle field numerically. It features a novel complex amplitude-based method for particle extraction, which overcomes the depth-of-focus problem and the speckle noise problem in digital holography.

This paper discusses various technical aspects in this digital holographic PIV system. The method for numerical hologram reconstruction and a complex amplitude-based method for particle extraction are introduced. Velocity extraction based on particle centroid data and decomposed 2D correlation is described. At last we present the preliminary result of the benchmark experiment using a water jet.

2. DIGITAL HOLOGRAPHIC PIV SYSTEM

Figure 1 shows the optical setup for hologram recording in our digital holographic PIV system. To minimize spatial resolution requirement in hologram recording, in-line holography is adopted, where the unscattered part of the illumination wave serves as the reference wave to interfere with the scattered waves by the particles. The 514-nm coherent light from an Argon laser (Coherent Innova 90) is used for hologram recording. To enable two-frame, double-exposure PIV, the laser beam is modulated by an acousto-optic Bragg cell (IntraAction AOM 404-A1) to generate a pair of briefly separated light pulses at an adjustable frequency. The pulsed laser beam is then collimated to form an illumination beam for in-line hologram recording. The illumination area is shaped by a square aperture of $1\text{ cm} \times 1\text{ cm}$ to fit the size of image sensor. A 12-bit CCD camera (PCO SensiCam) is used to record the digital holograms. This camera has 1280×1024 pixels of size $6.7\text{ }\mu\text{m}$, and the total CCD target area is $8.6\text{ mm} \times 6.9\text{ mm}$. To ensure proper timing in the experiment, an internal timing board (Keithely CTM-10) and an external pulse generator (BNC model 555) are used to synchronize the Bragg cell and the digital camera.

Figure 2 illustrates the data flow chart for hologram processing in the current system. The first step is hologram preprocessing to correct inhomogeneous illumination and to remove background noise. Then the digital holograms are numerically reconstructed to obtain the total reconstruction wave in the image volume. Next, information about tracer

particles such as 3D position and size are extracted from the total reconstruction wave using a complex amplitude-based method. Two sets of particles are retrieved from two briefly spaced exposures, respectively. Finally the particle data is processed by a decomposed correlation method to obtain the 3D velocity field.

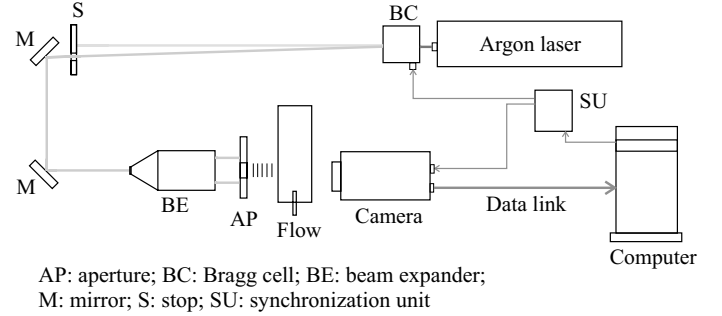


Fig. 1. Optical setup for hologram recording.

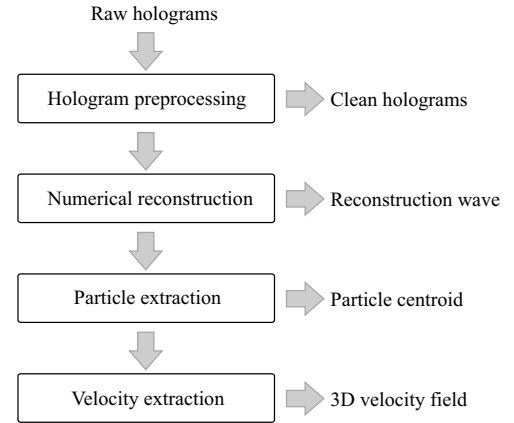


Fig. 2. Data flow chart for hologram processing.

2.1 Digital hologram recording

Solid-state image sensor such as CCD or CMOS image sensor consists of a matrix of neighboring sensing elements called pixels. The voltage readout of each pixel is proportional to the *integrated* light intensity on that pixel. Therefore, in digital holography a hologram is essentially the discrete sampling of a *low-pass filtered* intensity function. Denoting Δ as the pixel size and N as the number of pixels of a CCD sensor, the discrete intensity function (the hologram) can be written as

$$I_H(m, n) = I_{w,lp}(\xi, \eta) \cdot \delta(\xi - m\Delta, \eta - n\Delta) = \{I_w(\xi, \eta) \otimes [rect(\xi/\Delta) \cdot rect(\eta/\Delta)]\} \times \delta(\xi - m\Delta, \eta - n\Delta) \quad (1)$$

where m and n are integers in $[1, N]$; $I_{w,lp}$ and I_w are the filtered and the original intensity functions, respectively; $rect$ is the rectangular box function, and \otimes denotes convolution.

According to the sampling theorem, the Nyquist wave number of a CCD sensor is π/Δ ($2\pi \cdot 1/2\Delta$). Even in in-line

holography this resolution is not sufficient to fully resolve the spectrum of a continuous hologram. However, as defined in Eq. (1), the discrete sampling is actually performed with the filtered intensity function $I_{w,lp}$ instead of the original intensity function I_w . Due to convolution with the rectangular box function, the bandwidth of $I_{w,lp}$ is limited and the maximum wave number is approximately equal to $2\pi/\Delta$. As a result, although the recording resolution is low, the aliasing error caused by under-sampling is always minor in digital holograms.

2.2 Reconstruction of digital holograms

(1) Hologram preprocessing

With traditional holography, holograms cannot be bettered once they are recorded and developed, and hence any imperfection in recording will directly deteriorate the hologram reconstruction. This drawback can be overcome in digital holography because various imaging processing techniques can be applied on digital holograms to achieve the optimization of reconstruction images. For example, the fringe contrast of a hologram can be improved by image equalization; the inhomogeneous illumination in recording can be corrected by background subtraction; and the noise fringes caused by dirt or other objects can be eliminated through appropriate filtering operation. Shown in Fig. 3 are the holograms after subsequent preprocessing steps. The left picture is the raw hologram; the middle one is the hologram after local-mean subtraction (LMS); and the right one is the hologram after both LMS filtering and the spectrum-selection (SS) filtering.

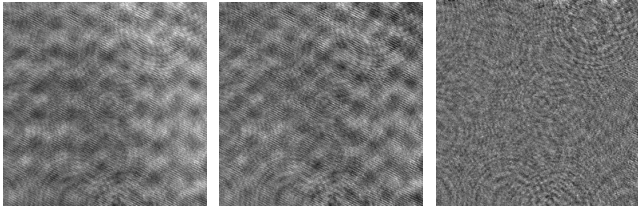


Fig. 3. Holograms after subsequent preprocessing steps.

(a) **Local-mean subtraction filter:** With this filter, the gray level at each pixel is subtracted by the local average in a small square window. In the wave number domain, the filter is defined by

$$I_{H,lms}(u, v) = I_H(u, v) \cdot [1 - \text{sinc}(W \cdot u) \cdot \text{sinc}(W \cdot v)] \quad (2)$$

where W is the size of the averaging window. The local-mean subtraction filter is essentially a high-pass filter, and therefore it also removes the dc component in hologram reconstruction.

(b) **Spectrum-selection filter:** The apparent background fringes in the raw holograms are probably caused by the beam expander and the cover glass in front of the CCD sensor. The regular pattern of these fringes results in a few particularly strong wave-number components in the power spectrum of the holograms. Therefore, a spectrum-selection filter is designed to detect those wave-number components in the power spectrum and then change their Fourier coefficient to zero.

(2) Numerical reconstruction

Conventionally, the optical reconstruction is performed by placing the holograms back into the recording setup and illuminating by the same coherent reference wave. The diffraction of the reference wave by the hologram yields the total reconstruction wave consisting of four terms:

$$U = |R|^2 + |O|^2 + R^*O + RO^*, \quad (3)$$

where R is the reference wave, O is the object wave, R^*O is the virtual image wave and RO^* is the real image wave.

In digital holography, hologram reconstruction can be performed numerically by applying scalar diffraction theory. A simple model for reconstruction in digital holography is outlined in Fig. 4. The hologram $I_H(\xi, \eta)$ is located at the plane $z = 0$, and the reconstruction wave $U(x, y)$ at any transverse plane is given by Rayleigh-Sommerfelds diffraction formula,

$$U(x, y, z) = \frac{1}{j\lambda} \iint I_H(\xi, \eta) R(\xi, \eta) \times \frac{\exp(jkr)}{r} \cos \Theta d\xi d\eta \quad (4)$$

where $R(\xi, \eta)$ is the reference wave used for illuminating the hologram plane. r is the distance from a given point in the hologram plane to a point in the reconstruction plane. $\cos \Theta$ is the obliquity factor that can be approximated by $\cos \Theta \equiv 1$ where the accuracy is to within 5% if the angle Θ does not exceed 18° . Accepting the validity of the Fresnel approximation, the diffraction integral in Eq. (4) becomes

$$U(x, y, z) = \iint I_H(\xi, \eta) R(\xi, \eta) \frac{\exp(jkz)}{j\lambda z} \times \exp\left\{\frac{jk}{2z}[(x-\xi)^2 + (y-\eta)^2]\right\} d\xi d\eta \quad (5)$$

where the total reconstruction wave may be regarded as a convolution of $I_H R$ with the kernel function h , which is given explicitly by

$$h_z(x, y) = \frac{\exp(jkz)}{j\lambda z} \exp\left\{\frac{jk}{2z}(x^2 + y^2)\right\} \quad (6)$$

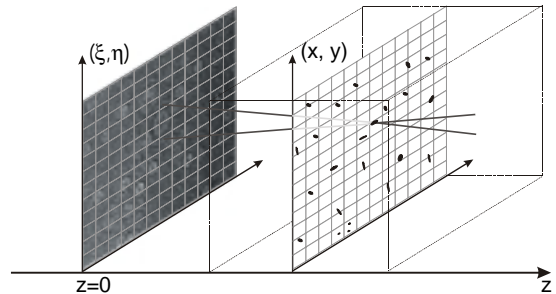


Fig. 4. Coordinate system in hologram reconstruction.

Applying the convolution theorem, the numerical implementation of the diffraction integral in Eq. (5) can be carried out efficiently by Fast Fourier Transform (FFT).

To reconstruct the 3D objects recorded by a hologram, the total reconstruction wave U in a series of transverse planes is computed. The intensity distribution in each reconstruction plane is equivalent to the photographic image focusing at that particular plane. This reconstruction scheme is the numerical implementation of the mechanical scanning that is often used in optical hologram reconstruction.

2.3 Extraction of particle information

In digital HPIV, the velocity field is deduced from the displacement of tracer particles in two briefly spaced exposures. Therefore, it is crucial to develop a robust and accurate method for extracting particles from the reconstructed 3D image field. Traditional particle extraction methods are solely based on intensity information since sensors used for interrogating the reconstructed image field in optical reconstruction only respond to intensity. By contrast, with numerical reconstruction the complex amplitude of the reconstruction wave is calculated using the diffraction integral and thereby both intensity and phase data are immediately available. This unique feature of numerical reconstruction extends particle extraction to the complex domain and therefore enables more effective tackling of the depth-of-focus problem and the speckle noise problem that are intrinsic in particle holography.

(1) Particle 3D images

In hologram reconstruction, particle 3D images are obtained from the intensity of the total reconstruction wave U . First in each scanning plane the 2D objects are found using image processing techniques including thresholding, boundary tracing, and object labeling. Then particle 3D images are constructed by clustering the overlapped 2D objects on adjacent planes.

Due to the small aperture of digital holograms, the reconstructed particle 3D images show remarkably large depth of focus. Simulation results have shown that the depth of focus of particle intensity images is more than 40 particle diameters. Such a large depth of focus severely restricts the depth resolution of intensity-based particle extraction.

(2) PECA method

Based on digital hologram recording and numerical hologram reconstruction, we have developed a novel method for particle extraction using complex amplitude (PECA). This method uses the complex amplitude of the total reconstruction wave to extract particle depth position. Particle transverse positions are then obtained directly from the intensity image in the particle in-focus plane.

It was found that, in the reconstruction of particle holograms formed by forward scattering, the imaginary part of the object wave vanishes at the in-focus plane of the particles. As a result, the variance of the imaginary part of U , which is defined in a transverse plane for the pixels belonging to the 2D image of a particle, is the minimum at the in-focus plane of that

particle. This so-called dipping characteristic of the total reconstruction wave is demonstrated in Fig. 5, where the variance of $Im(U)$ in the planes near a particle is plotted against z . The curve displays the dipping shape with its minimum at the in-focus position of $z = 27.585$ mm.

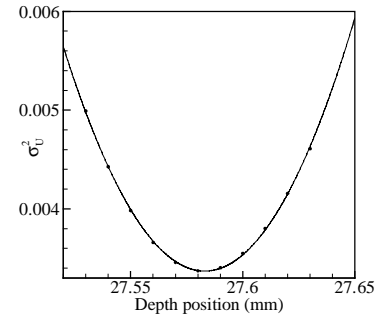


Fig. 5. The dipping characteristic of $Im(U)$.

By virtue of the dipping characteristic the PECA method can achieve very high accuracy in extracting particle depth positions regardless of the small numerical aperture in digital hologram recording. Fig. 6 shows the calibration result using synthesized holograms. The particle depth position obtained by the PECA method is compared with the known position of the particles, and the histogram of the depth error is calculated. It is found that the average depth error of the PECA method is less than the particle diameter even in presence of high particle number densities. More detail about the PECA method can be found in Pan and Meng [13].

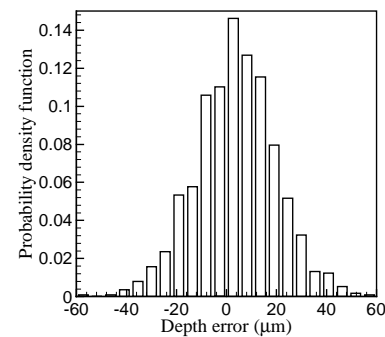


Fig. 6. Depth error of the PECA method.

(3) Speckle noise

Speckle noise problem is intrinsic in particle holography especially in holographic PIV due to dense particle distribution in the sample volume. It was found that, in the reconstruction of particle holograms, the speckle noise level increases proportionally with particle number density and sample volume depth [14]. To make things worse, the characteristic speckle size is comparable with the particle image size no matter how much the recording resolution is. This makes particle recognition difficult in densely populated particle fields, where the intensity level of speckle noise is comparable with the average intensity of particle images. Consequently, a lot of

“false particles” will be generated in particle extraction and deteriorate the accuracy of subsequent velocity computation.

To overcome the speckle noise problem, we have implemented an effective method in our digital holographic PIV system by virtue of flexible numerical reconstruction scheme and the dipping characteristic of particles. This method consists of two steps. The first step is suppressing speckle noise in hologram reconstruction and the second step is detecting speckles in particle extraction.

(a) **Suppressing speckle noise:** In reconstruction of in-line particle holograms, the real image wave of out-of-focus particles and the virtual image wave are two major sources of speckle noise. For far-field particle holography, the magnitude of virtual image wave is very weak in the region where particles are extracted. Therefore, the contribution of virtual image wave to the speck noise can be effectively suppressed if the directed transmitted wave (the dc term) is not presented in the reconstruction so that the interference between the two waves is avoided. In numerical reconstruction the directed transmitted wave is the dc term in the total reconstruction wave U , and can be easily removed. As a result, the speckle noise level is decreased, and the real image wave of out-of-focus particles becomes the dominant source of the speckle noise.

(b) **Detecting speckles:** Due to their comparable size and intensity level, speckles and particles cannot be differentiated in intensity images. But it is possible to distinguish particles and speckles in the complex amplitude domain. We know that speckles are formed by the summation of individual real image wave of out-of-focus particles, and the summation can be viewed as a 2D random walk in the complex plane. This random process is unlikely to produce the dipping pattern of the complex amplitude of U near a speckle. Therefore the dipping shape of the variance of $Im(U)$ only appears in the neighborhood of particles, and speckle can be detected by checking if a 3D object constructed from intensity images have the dipping characteristic.

2.4 Extraction of velocity field

A decomposed 2D correlation method has been developed for velocity field extraction in digital holographic PIV. This method computes the 2D correlations on the projection images of a 3D particle field, and then combines the resulted 2D displacement vectors into a 3D one by matching the displacement on the common axis between any two 2D vectors. To enable correlation computation in the frequency domain, virtual particle images are generated using particle centroid coordinates and an arbitrary impulse response function.

Assuming that particle 3D positions have been extracted from two consecutive frames (holograms), respectively, the particle field in each frame can be interpreted as the output of a linear system with particle position input $P(x, y, z, t)$ and impulse response function $h(x, y, z, t)$:

$$F(x, y, z, t) = P(x, y, z, t) \otimes h(x, y, z, t) \quad (7)$$

with $P(x, y, z, t) = \sum_i \delta(x - x_i, y - y_i, z - z_i, t)$

where \otimes is the convolution operator and δ is the Dirac function.

To compute the cross-correlation of two frames F_A and F_B , we can assume that the impulse response h of a particle is an isotropic 3D Gaussian function:

$$G_i(x, y, z) = A_i \cdot \exp\left[-\frac{(x - x_i)^2 + (y - y_i)^2 + (z - z_i)^2}{2R_i^2}\right] \quad (8)$$

where the 3D coordinates (x_i, y_i, z_i) of the particle are obtained from hologram reconstruction. The amplitude A_i and the spot size R_i can be either obtained from particle extraction or arbitrarily selected in velocity computation.

We know that the convolution of two Gaussian functions is also a Gaussian function. Therefore, the cross-correlation of two particles G_i and G_j , taken respectively from particle field F_A and F_B , would be (Pereira and Gharib 2002)

$$R_{G_i G_j} = A_i A_j \left(\frac{\sqrt{2\pi} R_i R_j}{\sqrt{R_i^2 + R_j^2}} \right)^3 \times \exp\left[-\frac{(x + x_i - x_j)^2 + (y + y_i - y_j)^2 + (z + z_i - z_j)^2}{2(R_i^2 + R_j^2)}\right] \quad (9)$$

Obviously, Eq. 9 can be decomposed into the multiplication of three 2D cross-correlations. Since the complete cross-correlation of two particle fields is simply the sum of cross-correlation of every pair of particles, we can recover the maximum 3D cross-correlation from the cross-correlation of their 2D projections. The corresponding 3D displacement between two particle fields can also be obtained from the peak location of the 2D correlations.

To use the decomposed correlation method for velocity extraction, particle 3D images are first generated from the convolution of particle positions $P(x, y, z, t)$ and the isotropic 3D Gaussian function impulse response $G(x, y, z)$. Then three projection images of the particle field are created for each frame, namely x - y , y - z and z - x projection. The 2D cross-correlations of the three pair of projection images are computed to obtain the 2D displacement in each projection plane. Due to random error of particle positions, it is possible that the highest 2D-correlation peak may not correspond to the actual 3D-correlation peak. Therefore, from each 2D correlation a number of peaks need to be collected for the construction of 3D displacement vector.

Since there is a common axis between any two projections, the 2D displacement obtained from both projections should have the same displacement on the common axis. This is a natural constraint that can be used to directly construct the 3D displacement vector, saving an additional 3D correlation which cannot be computed in the frequency domain.

3. EXPERIMENTAL RESULTS

The digital in-line holographic PIV system described above is tested with the measurement of a water jet. The scheme of the experimental setup is shown in Fig. 7. The gravity-driven flow issued from a vertical tube (1.4 mm ID, stainless steel) forms the jet in the middle of a glass tank ($10 \times 50 \times 50 \text{ mm}^3$). A small reservoir is put on top of the glass tank to increase the downstream distance so that the flow in the near field of the jet is not affected by any free-surface effect. During the experiment, the water is seeded with neutrally buoyant tracer particles (Dantec PSP20, 20 μm diameter) at a seeding density of about 24 particle/ mm^3 . The Reynolds number based on jet exit velocity and jet diameter is about 140.

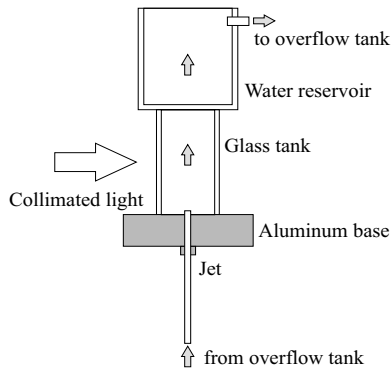


Fig. 7. Experimental setup for the water jet flow.

Since no lens is used in hologram recording, the size of the CCD sensor decides the cross-section area of the sample volume. In this experiment, the maximum sample volume is $8.6 \times 6.9 \times 10 \text{ mm}^3$. Two-frame, double-exposure holograms were recorded by the digital camera at a frame rate of 4 pairs/sec. The light pulses produced by the Bragg cell is synchronized with the camera and the pulse width was set at 5 μs . The delay between pulses in each pair was 20 ms in the current measurement.

The digital holograms are processed according to the procedure depicted in Fig. 2. Shown in Fig. 8 is an example of the numerically reconstructed image of tracer particles (double exposure) in an area of about 1.3 mm^3 . The image quality is superior to that in optical in-line holography because the twin-image effect is effectively suppressed by filtering the dc component in numerical hologram reconstruction.

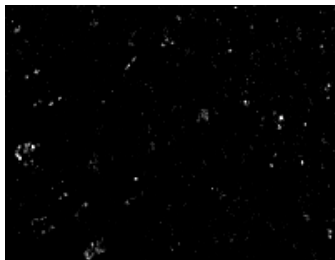


Fig. 8. Reconstructed image of tracer particles.

The decomposed 2D correlation method is used to extract the 3D velocity field on planes stacked along three orthogonal directions. Commercial PIV software (proVision, IDT Inc.) was used to process the projection images. Shown in Fig. 9 is the vector map on three x - y cross-sections (1 mm apart) in the sample volume. Each map covers an area of about $3 \times 3 \text{ mm}^2$ in the immediate vicinity of the jet exit (about $1/3$ jet diameter downstream). The jet body and the induced flow around the jet are clearly identified in the velocity maps.

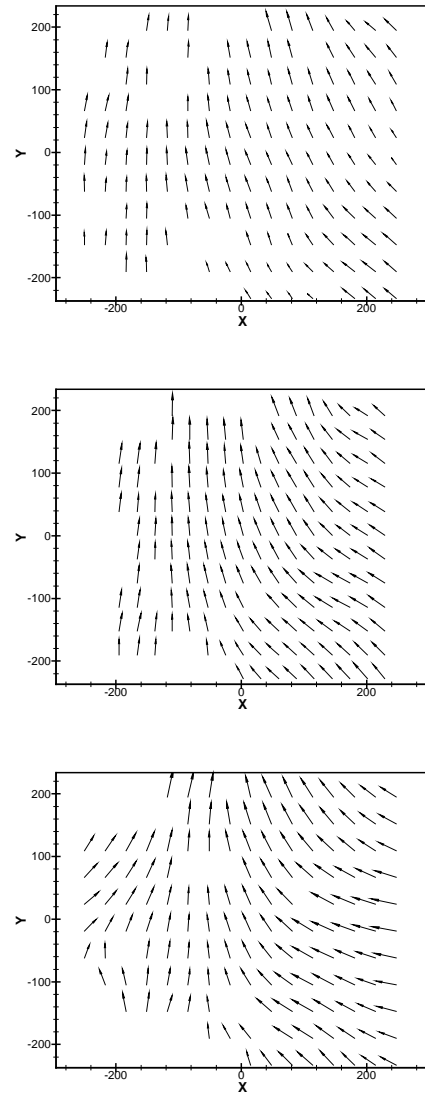


Fig. 9. Simultaneous velocity vector map on three x - y planes 1 mm apart.

The velocity vectors on y - z planes and z - x planes were also obtained, but the errors are significant due to the uncertainty in depth position measurement. We expect that, through further improvement, the decomposed correlation method will be able to tolerate larger depth error such that the correct velocity vectors can be obtained in the projections involving the z -axis. It is important to point out that better results can be obtained by

using CCD sensors with smaller pixels since the uncertainty of particle depth positions decreases as the recording resolution improves.

4. CONCLUSION

We have developed a simple digital in-line holographic PIV system for 3D measurement of turbulent and multiphase flow. This system records in-line holograms of tracer particles directly on a digital camera and reconstructs the 3D particle field numerically. The numerical hologram reconstruction is based on the Fresnel approximation of the Rayleigh-Sommerfelds diffraction formula. To improve the quality of reconstruction images, background noise and inhomogeneous illumination are removed from the digital holograms prior to the numerical reconstruction. A novel complex amplitude-based method has been developed for particle extraction from the reconstruction wave. With this method, we are able to overcome two major problems in digital particle holography, namely the depth of focus problem and the speckle noise problem. Velocity extraction is based on particle centroid data obtained from two briefly separated frames. A decomposed correlation method is utilized for velocity extraction.

The system has been tested by a water jet flow, and the preliminary result is presented. The velocity vectors obtained from the x - y projections are satisfactory. However, further improvement of the velocity extraction method is necessary in order to produce truly 3D velocity vectors.

REFERENCES

1. Prasad, K., and Jensen, K., 1995, "Scheimpflug stereocamera for particle image velocimetry in liquid flows," *Appl. Opt.*, **34**, pp. 7092-7099.
2. Bruecker, C., 1997, "3D scanning PIV applied to an air flow in a motored engine using digital high-speed video," *Meas. Sci. Technol.*, **8**, pp. 1480-1492.
3. Kahler, C. J., and Kompenhans, J., 2000, "Fundamentals of multiple plane stereo particle image velocimetry", *Exp. in Fluids*, **29**, pp. S70-S77.
4. Pereira, F., and Gharib, M., 2002, "Defocusing digital particle image velocimetry and the three-dimensional characterization of two-phase flows," *Meas. Sci. Technol.*, **13**, pp.683-694.
5. Hinsch, K. D., 2002, "Holographic particle image velocimetry," *Meas. Sci. Technol.*, **13**, pp. R61-R72.
6. Barnhart, D. H., Adrian, R. J., Meinhart, C. D., Papen G. C., 1994, "Phase-conjugate holographic system for high-resolution particle image velocimetry," *Appl. Opt.*, **33**, 7159-7169.
7. Meng, H, Hussain, F, 1995, "In-line Recording and Off-axis Viewing (IROV) technique for holographic

particle velocimetry," *Appl. Opt.*, **34**, pp.1827-1840.

8. Zhang, J, Tao, B, Katz, J, 1997, "Turbulent flow measurement in a square duct with hybrid holographic PIV," *Exp. in Fluids*, **23**, pp.373-381.
9. Pu, Y., Meng, H., 2000, "An advanced off-axis holographic particle image velocimetry (HPIV) system," *Exp. in Fluids*, **29**, 184-197.
10. Meng, H., Hussain, F., 1991, "Holographic particle velocimetry, a 3D measurement technique for vortex interactions, coherent structures and turbulence," *Fluid Dynamics Research*, **8**, 33-52.
11. Owen, R. B., Zozylyya, A. A., 2000, "In-line digital holographic sensor for monitoring and characterizing marine particulates," *Opt. Eng.*, **39**, pp. 2187-2197.
12. Onural, L., Scott, P. D., 1987, "Digital decoding of in-line holograms," *Opt. Eng.*, **26**, pp. 1124-1132.
13. Pan, G., and Meng, H., 2002, "Digital holography of particle fields: reconstruction using complex amplitude," *Appl. Opt.*, submitted.
14. Meng, H., Anderson, W. L., Hussain, F., and Liu, D., 1983, "Intrinsic speckle noise in in-line particle holography," *J. Opt. Soc. of Am. A*, **10**, 2046-2058.